Metastability limit in the supercooled liquid state and its implications for glass formation and crystallization

Kengo Nishio *

Materials DX Research Center, National Institute of Advanced Industrial Science and Technology (AIST), 1-1-1 Umezono, Tsukuba, Ibaraki 305-8568, Japan

(Received 1 July 2026; accepted 27 October 2026; published 17 November 2026)

A supercooled liquid is thermodynamically unstable relative to the crystal, yet it can persist for long times near the melting temperature. Its lifetime, however, decreases with decreasing temperature. In some systems, a metastability-limit temperature has been reported, below which the system crystallizes without forming a supercooled liquid state. Whether such a limit is universal or material specific remains an open question. In this study, we use molecular dynamics simulations and the p_3 code to show that a metastability limit exists in a model Laves-phase-forming alloy. In isothermal annealing below its metastability-limit temperature, local crystalline domains form immediately throughout the system. This suggests that controlling crystallization below this temperature may offer a route to tuning the physical properties of glassy materials via the formation of nanoscale crystalline regions. During cooling at rates close to the critical cooling rate, crystallization initiates near the metastability-limit temperature. This indicates that the metastability limit influences the competition between glass formation and crystallization. Consideration of the system-size dependence of metastability suggests that the metastability-limit temperature of a microscopic system provides a measure of the stability of liquidlike regions in a macroscopic system. Below this temperature, liquidlike regions larger than the microscopic system are unlikely to exist in a metastable equilibrium state. We also discuss the implications of a metastability limit for defining glass. Originally proposed as a possible resolution of the Kauzmann paradox, the metastability limit has broader implications for glass formation, the control of material properties via structural design, and the definition of glass.

DOI: 10.1103/wh25-ltlc

I. INTRODUCTION

A liquid below its melting temperature is thermodynamically unstable relative to the crystal. However, it can persist in a metastable equilibrium state for some time before transforming into a stable crystal [1–4]. This state is referred to as a supercooled liquid. Near the melting temperature, the supercooled liquid state can persist for long times, but its lifetime decreases as the temperature is lowered. In some systems, a metastability limit has been reported, which is characterized by a temperature below which liquid crystallizes without forming a supercooled liquid state [4–11]. A metastability limit implies that the supercooled liquid state does not exist below the corresponding temperature. We denote this temperature as T_{ml}. The existence of a metastability limit was originally proposed as a possible resolution of the Kauzmann paradox [12]. This limit may have important implications for glass formation and, more broadly, for the definition of glass. Since a universally accepted definition of glass remains elusive [13–16], we use the term *glass* here to refer to noncrystalline solidlike materials with liquidlike disordered structures, unless otherwise noted. Despite its potential implications, it remains an open question whether a metastability limit is universal or specific to certain classes of materials [4–7,17].

Glasses are typically formed by cooling liquids. For a glass to form, crystallization must be suppressed kinetically, as crystals are thermodynamically stable below the melting temperature. Since liquids tend to crystallize under slow cooling, glass formation requires sufficiently rapid cooling to freeze the liquid structure before crystallization occurs. The minimum cooling rate required to avoid crystallization is called the critical cooling rate, which serves as a key measure of glass-forming ability. If a metastability limit exists, then it imposes a fundamental constraint on the existence of the supercooled liquid state, thereby influencing the conditions under which glasses form. Therefore, understanding the metastability limit is important for elucidating glass formation.

To gain fundamental insights into the physics of supercooled liquids, Lennard-Jones models have been extensively studied [18–29]. One representative system is the Wahnström binary mixture [30], which consists of two types of atoms: large (L) and small (S). Previous studies have shown that supercooled liquids in this model can crystallize into LS_2 Laves phases such as C14 and C15 [27–29]. The Wahnström mixture can therefore be regarded as a model for alloys that

*Contact author: k-nishio@aist.go.jp

Published by the American Physical Society under the terms of the Creative Commons Attribution 4.0 International license. Further distribution of this work must maintain attribution to the author(s) and the published article's title, journal citation, and DOI.

form Laves phases [31,32]. Our recent study has shown that supercooled liquids in this alloy are populated with numerous crystal-like clusters and that these clusters connect to form superclusters [29]. The presence of such crystal-like superclusters may indicate the existence of a metastability limit. Although one-component Lennard-Jones systems are known to exhibit a metastability limit [10], it is not known whether such a limit exists in the Wahnström alloy.

In this work, to gain insight into the nature of the metastability limit, including whether it is universal or material-specific, we investigate the metastability limit in the Wahnström alloy, a model Laves-phase-forming system. To this end, we perform molecular dynamics simulations and analyze local structures using the p_3 code [29,33–37]. The remainder of this paper is organized as follows. In Sec. II, the Wahnström model alloy, the molecular dynamics scheme, and the structural analysis method based on the p_3 code are described. Section III distinguishes between thermodynamic and kinetic metastability limits and clarifies that the metastability limit investigated in this work is a kinetic metastability limit. We explain in Sec. IV how a supercooled liquid state is identified from the time evolution of the potential energy. Our main results are reported in Sec. V, where we show that (1) a metastability limit exists in the Wahnström alloy; (2) $T_{\rm ml}$ depends on composition; (3) in isothermal annealing below $T_{\rm ml}$, local crystallization sets in immediately throughout the system; (4) $T_{\rm ml}$ depends on the system size; and (5) during cooling at rates close to the critical cooling rate, crystallization initiates near $T_{\rm ml}$. We also discuss the implications of the system-size dependence of $T_{\rm ml}$ from the perspective of the local nature of metastability. In Sec. VI, the implications of a metastability limit for defining glass are discussed. Finally, our findings are summarized in Sec. VII.

II. METHODOLOGY

A. Wahnström model alloy

We examine the Wahnström model as a representative system that forms a Laves phase. Since Laves phases are observed in a wide range of materials, including Cr-, Cu-, Fe-, Mg-, Nb-, Ni-, Ti-, and Zr-based alloys [31], as well as in colloidal mixtures [32], the results based on this model are expected to provide a useful reference point for comparative studies on supercooled liquids and glass formation in other Laves-phase-forming systems.

The Wahnström model consists of large (L) and small (S) atoms interacting via the cut-and-shifted Lennard-Jones potential,

$$\Phi_{\alpha_i\alpha_j}(r_{ij}) = \begin{cases} \phi_{\alpha_i\alpha_j}(r_{ij}) - \phi_{\alpha_i\alpha_j}\left(r^c_{\alpha_i\alpha_j}\right) & \left(r_{ij} < r^c_{\alpha_i\alpha_j}\right) \\ 0 & \left(r^c_{\alpha_i\alpha_j} \leqslant r_{ij}\right) \end{cases}, \quad (1)$$

where

$$\phi_{\alpha_i\alpha_j}(r_{ij}) = 4\epsilon_{\alpha_i\alpha_j}\left(\left(\frac{\sigma_{\alpha_i\alpha_j}}{r_{ij}}\right)^{12} - \left(\frac{\sigma_{\alpha_i\alpha_j}}{r_{ij}}\right)^{6}\right). \quad (2)$$

Here α_i represents the chemical identity of atom i (L or S), and r_{ij} is the distance between atoms i and j. $r^c_{\alpha_i\alpha_j} = 2.5\sigma_{\alpha_i\alpha_j}$ is the cutoff distance. $\sigma_{SS} = \sigma_{SL}/1.1 = \sigma_{LL}/1.2$, $\epsilon_{SS} = \epsilon_{SL} = \epsilon_{LL}$, and $m_S = m_L/2$ [30]. Hereafter, we use the L-atom Lennard-Jones reduced units: length σ_{LL}, energy ϵ_{LL}, temperature ϵ_{LL}/k_B, pressure $\epsilon_{LL}/\sigma^3_{LL}$, time $\sqrt{m_L\sigma^2_{LL}/\epsilon_{LL}}$, and cooling rate $\sqrt{\epsilon^3_{LL}/m_L\sigma^2_{LL}k^2_B}$.

Unless otherwise specified, we examine systems composed of 10 000 atoms. In one system, 3333 L atoms and 6667 S atoms are present, yielding an L-atom fraction of $x_L = 0.333$. Although this composition is not strictly stoichiometric, the deviation is small. Therefore, we regard it as nominally stoichiometric. Two other systems have $x_L = 0.224$ (2240 L atoms and 7760 S atoms) and $x_L = 0.520$ (5200 L atoms and 4800 S atoms). The system with $x_L = 0.224$ corresponds to the eutectic composition between the S-atom fcc phase and the C14 LS_2 phase [38], while the system with $x_L = 0.520$ corresponds to the eutectic composition between the L-atom fcc phase and the C14 LS_2 phase.

B. Molecular dynamics simulations

We performed molecular dynamics simulations in the NPT ensemble using LAMMPS [39,40]. The timestep was set to 0.002. Following Ref. [20], the pressure was set to 10. The thermostat and barostat damping constants were set to 0.1 and 10, respectively.

To examine whether a metastability limit exists, the system was equilibrated at the liquidus temperature [38] for at least 1000 time units. Equilibration was confirmed by the absence of any systematic drift in the potential energy. Configurations sampled from the equilibrated trajectory at intervals of 1000 time units were then instantaneously quenched to each target temperature to monitor their subsequent temporal evolution.

To study glass formation, the liquid equilibrated at the liquidus temperature was cooled down to $T = 0.500$ using five different cooling rates, 10^{-4}, 10^{-5}, 10^{-6}, 10^{-7}, and 10^{-8}. The temperature was decreased stepwise, with a temperature increment of $\Delta T = 0.001$. At each step, the target temperature was instantaneously lowered, after which the system was allowed to evolve at constant temperature. At each temperature, the structure was analyzed using the final configuration. For reference, when the Lennard-Jones parameters for the L atoms are taken to be those of argon, the slowest cooling rate 10^{-8} corresponds to approximately 0.5×10^6 K/s.

C. Structural analysis based on the p_3 code

The crystallinity of the system was quantified based on the p_3 code [33–36]. Specifically, we focused on loose-crystalline bipyramids introduced in Ref. [29]. These calculations were performed using the Voronoi and LCS software packages [29,35,37]. Because the definition of loose-crystalline bipyramids relies on crystalline bipyramids, their derivatives, Frank-Kasper Z16* clusters, and icosahedral IC3 clusters, we first describe these structures.

1. Crystalline bipyramids and their derivatives

A bipyramid is a cluster consisting of two atoms bonded to each other and their common neighbors [36]. The two bonded atoms are called apex atoms, while the common neighbors are called base atoms. A bipyramid with n base atoms is called an n-gonal bipyramid. A crystalline bipyramid is a

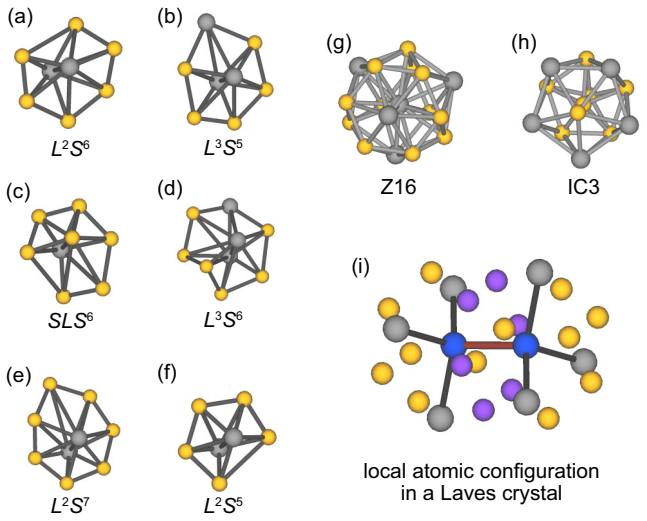


FIG. 1. Cluster structures. (a) Crystalline bipyramid, [(b)–(f)] its derivatives, (g) Z16 cluster, (h) IC3 cluster, and (i) local configuration in a Laves crystal. Gray and orange spheres represent L and S atoms, respectively. In panel (i), a connectivity-six loose-crystalline bipyramid composed of two blue L atoms and six purple S atoms is highlighted. This bipyramid is a crystalline bipyramid, which is a special case of a loose-crystalline bipyramid. Bars represent apex bonds; the red bar indicates the apex bond of the highlighted bipyramid, to which six bars are connected.

hexagonal bipyramid consisting of two apex L atoms and six base S atoms [Fig. 1(a)]. LS_2 Laves crystals consist of such bipyramids connected through shared apex atoms [21,24,41].

Using the p_3 code, a crystalline bipyramid is encoded as $LLSSSSSS$ [24,36]. The order of the letters (two Ls followed by six Ss) reflects the spatial arrangement of the species: The two L atoms occupy the apexes, while the base consists of six S atoms. For a more compact representation, this code can be abbreviated as L^2S^6. The crystalline bipyramid is represented by 1551 in the Honeycutt-Anderson index [42], although this index does not distinguish chemical species.

The bond between the apex L atoms in an L^2S^6 bipyramid is called an L^2S^6 apex bond. This bond is referred to as an FK bond in Ref. [21]. In the C14 Laves crystal, the apex bonds form a tetrahedral network that is isostructural with the hexagonal diamond lattice, while in the C15 Laves crystal they form a network isostructural with the cubic diamond lattice.

Five derivatives can be obtained from the L^2S^6 bipyramid [36], each by a single modification:

(1) Replacing one S atom with an L atom yields L^3S^5 [Fig. 1(b)].

(2) Replacing one L atom with an S atom yields SLS^6 [Fig. 1(c)].

(3) Adding one L atom yields L^3S^6 [Fig. 1(d)].

(4) Adding one S atom yields L^2S^7 [Fig. 1(e)].

(5) Removing one S atom yields L^2S^5 [Fig. 1(f)].

2. Z16* clusters

A Z16 cluster consists of four crystalline bipyramids connected through a shared apex atom [Fig. 1(g)]. LS_2 Laves crystals are composed of Z16 clusters connected through shared crystalline bipyramids. A cluster is called a Z16* cluster if it has the same atomic connectivity as a Z16 cluster, independent of the species identity of its constituent atoms. Z16* clusters thus include Z16 clusters as a subset. Z16* clusters are found in supercooled liquids, and a higher population of these clusters leads to faster crystallization [29].

For reference, the Z16 cluster is encoded using the p_3 code as $@5^3(65)^35^66; LS^3(LS)^3S^6L$. Here, the first part, $@5^3(65)^35^66$, represents the atomic connectivity, while the second part, $LS^3(LS)^3S^6L$, specifies the chemical identity of its constituent atoms (L or S). The Z16* cluster is encoded as $@5^3(65)^35^66$.

3. IC3 clusters

An IC3 cluster is a special case of an icosahedral cluster, which consists of eight S atoms and five L atoms [Fig. 1(h)]. The five L atoms form a pentagonal ring. IC3 clusters are located along the fivefold symmetry axis of a fivefold twin formed by joining five C15 Laves crystals [24]. In this twin, pentagonal rings of apex bonds are stacked at the center. These rings arise from the pentagonal rings in the central IC3 clusters. IC3 clusters are found in supercooled liquids, and a higher population of these clusters leads to faster crystallization [29]. For reference, the IC3 cluster is encoded as $@5^{12}; S^7L^5S$.

4. Loose-crystalline bipyramids

The following bipyramids are structurally related to LS_2 Laves crystals: crystalline bipyramids, their derivatives, hexagonal bipyramids contained in Z16* clusters, and bipyramids whose apex L atoms belong to IC3 clusters. Loose-crystalline bipyramids are defined on the basis of these bipyramids. Although each bipyramid individually resembles a local crystalline motif, the manner in which these bipyramids are connected is often noncrystalline. In Laves crystals, bipyramids connected through a shared apex atom have apex bonds that form approximately a tetrahedral angle, $\theta_i = \cos^{-1}(-1/3) \approx 109^\circ$. In contrast, the corresponding angles in supercooled liquids frequently deviate significantly from this ideal tetrahedral value. To exclude strongly distorted configurations, a criterion is imposed on the apex-bond angles: An apex-bond angle θ is regarded as tetrahedral if it satisfies $|\theta - \theta_i| < 15^\circ$ [29]. The threshold of 15° is chosen such that 99% of the apex-bond angles in the C14 Laves crystal at the liquidus temperature satisfy this condition.

Loose-crystalline bipyramids are defined using a state-assignment procedure, where each bipyramid falls into one of three states: *on*, *off*, or *pending*. The procedure also identifies complete or partial pentagonal rings, as they form the core of fivefold twins, which have been shown to influence crystallization [29]. Starting from the *off* state for all bipyramids, the states are updated, and bipyramids in the *on* state are defined as loose-crystalline bipyramids. In each step, all state updates are applied simultaneously after evaluating all relevant bipyramids, so that the result does not depend on the processing order. The procedure is defined as follows:

(1)

(a) Initialize all bipyramids to the *off* state.

(b) Change the state of L^2S^6 bipyramids to *on*.

(2)

(a) Change the state of an *off*-state bipyramid to *pending* if its apex atoms are of element L and contained in the same IC3 cluster.

(b) Apply the bond-angle screening as follows:

(i) Change the state of a *pending*-state bipyramid to *off* if, for any *on*-state bipyramid sharing an apex atom with it, the angle between their apex bonds does not satisfy the tetrahedral criterion.

(ii) Change the state of a pair of *pending*-state bipyramids to *off* if they share an apex atom and the angle between their apex bonds does not satisfy the tetrahedral criterion.

(iii) Change the state of the remaining *pending*-state bipyramids to *on*.

(3)

(a) Change the state of *off*-state hexagonal bipyramids of each Z16* cluster to *pending*.

(b) Apply the bond-angle screening by repeating Step (2) (b).

(4)

(a) Change the state of *off*-state L^3S^5, SLS^6, L^3S^6, L^2S^7, and L^2S^5 bipyramids to *pending*.

(b) Apply the bond-angle screening by repeating Step (2) (b).

(5)

(a) Change the state of an *off*-state bipyramid to *pending* if each of its two apex atoms is shared as an apex atom with at least one *on*-state bipyramid.

(b) Apply the bond-angle screening by repeating Step (2) (b).

(6) Change the state of an *on*-state bipyramid to *off* if neither of its apex atoms is shared with any other *on*-state bipyramid.

(7) Bipyramids in the *on* state are loose-crystalline bipyramids.

(8) The following steps are then used to identify complete or partial pentagonal rings based on the bipyramids identified above.

(a) Repeat Step (5) (a).

(b) If five apex bonds of *on*- or *pending*-state bipyramids form a pentagonal ring consistent with the tetrahedral bond network, then the apex bonds of *on*-state bipyramids are regarded as forming a complete or partial pentagonal ring.

III. THERMODYNAMIC AND KINETIC METASTABILITY LIMITS

Several criteria have been proposed to characterize the instability of the supercooled liquid state [4–12,17]. The thermodynamic metastability limit is associated with the vanishing of the nucleation barrier [10–12]. However, even when the barrier remains finite, it can be sufficiently small that nucleation occurs without the formation of a supercooled liquid state. Thus, in practice, the instability is governed by kinetics. Kinetic instability can be characterized by the temperature at which the nucleation time falls below the structural relaxation time [4–9]. The kinetic instability characterized in this way was termed a kinetic spinodal in Ref. [4].

In the present study, we characterize kinetic instability in terms of the time evolution of the potential energy. To this end, we define the supercooled liquid state as a metastable equilibrium state exhibiting a stationary potential-energy regime in which the potential energy fluctuates around an approximately constant level. The lifetime of the supercooled liquid state is defined as the duration of this regime. When crystallization occurs without the formation of a supercooled liquid state, no stationary regime is observed and the lifetime is therefore zero. Even at fixed composition, temperature, and pressure, the lifetime can vary among trajectories because crystallization is stochastic. We therefore define the metastability-limit temperature T_{ml} as the temperature at which the probability that the system does not form a supercooled liquid state reaches 50%. Because trajectories that do not form a supercooled liquid state have a lifetime of zero, T_{ml} corresponds to the boundary at which the median lifetime changes from a finite value to zero. We refer to the kinetic instability characterized in this way simply as the metastability limit. Although this criterion is also kinetic, it differs from definitions based on the comparison between nucleation and structural relaxation times. In particular, our approach explicitly examines the formation of the supercooled liquid state.

IV. PIECEWISE-LINEAR MODEL

For a given trajectory, the lifetime of the supercooled liquid state is determined using the piecewise-linear model proposed in Ref. [29]. In this method, the time evolution of the potential energy is fitted to a piecewise-linear function $E(t)$ given by

$$E(t) = \begin{cases} E_0 & t \leqslant t_l, \\ E_0 + \alpha(t - t_l) & t_l < t, \end{cases} \tag{3}$$

where $\alpha < 0$, reflecting the decrease in potential energy as crystallization proceeds. The initial stationary region represents the supercooled liquid state, while the linear decrease reflects the progression of crystallization. The obtained value of t_l corresponds to the crystallization onset time and is taken as the lifetime of the supercooled liquid.

In Ref. [29], the piecewise-linear model was introduced as a systematic method for estimating the lifetime of a supercooled liquid state, thereby avoiding subjective visual inspection of the potential-energy trajectory. In that work, the model was applied to trajectories for which the formation of a supercooled liquid state was evident. In the present study, we use the same model to determine whether the trajectory forms a supercooled liquid state. Because this application was not examined in Ref. [29], the physical rationale and the procedure employed in the present work are described in the following sections.

A. Physical rationale

When the system is in a supercooled liquid state, the potential energy fluctuates around a characteristic energy level. After crystallization begins, the energy level around which the potential energy fluctuates decreases as crystal-like order develops. Immediately after the onset of crystallization,

this decrease may be approximated as linear in time. The piecewise-linear model represents the evolution of the energy level around which the potential energy fluctuates, rather than the instantaneous potential energy itself.

One limitation of the piecewise-linear model is that it does not capture the initial structural-relaxation process that occurs following the quench, which is unrelated to crystallization. The influence of this relaxation process on the fit depends on how the initial relaxation time compares with the crystallization onset time. When the initial relaxation time is much shorter than the crystallization onset time, the fitted piecewise-linear function is only weakly affected by the initial relaxation process. We note that the lifetime t_l is measured from the instant of the quench rather than from the completion of the initial relaxation. Accordingly, t_l includes the relaxation period before the system reaches the supercooled liquid state. However, in the case considered here, where the initial relaxation time is much shorter than the crystallization onset time, this overestimation is small. Note also that, in this case, our criterion that a supercooled liquid state is identified by a nonzero fitted lifetime is consistent with the physical interpretation that a sufficiently long stationary regime provides clear evidence that a supercooled liquid state has formed.

By contrast, when the initial relaxation and crystallization are not clearly separated in time, it is unclear whether a stationary regime, even if observed, should be interpreted as evidence for the formation of a metastable equilibrium state or merely as a transient feature of an evolving system. The present procedure might assign a nonzero lifetime in such cases. One might therefore argue that the procedure overestimates the lifetime of the supercooled liquid state. However, such an overestimation would make it more difficult to conclude that the system exhibits a metastability limit. Consequently, if a metastability limit is observed, then this observation cannot be attributed to such an overestimation.

B. Fitting procedure

The fitted function is obtained by minimizing the sum of squared residuals. The fitting range is determined from the parameters ϵ, w, and λ. Before defining these quantities in detail, we note that ϵ represents an estimate of the energy level around which the potential energy is expected to fluctuate if the system is actually in a supercooled liquid state. The parameter w characterizes the magnitude of the fluctuations, and the parameter λ controls how far the fitting range extends toward lower energies. From these parameters, we define $t_{\max}$ as the time beyond which the smoothed potential energy falls below $\epsilon - \lambda w$. The fitting range is then taken as $0 < t < t_{\max}$. Here, the smoothed potential energy is used to reduce the influence of thermal fluctuations on the determination of the fitting range and is obtained by averaging the potential energy over a time interval Δt. The value of Δt is determined iteratively. For a given Δt, the fitting range is determined, and the piecewise-linear function is fitted to obtain the parameters E_0, t_l, and α. If the condition $0.1w/|\alpha| \leqslant \Delta t \leqslant 0.2w/|\alpha|$ is not satisfied, then Δt is adjusted and the fitting procedure is repeated until the condition is satisfied. Unless otherwise stated, $\lambda = 1$. If a supercooled liquid state is actually present, then this choice restricts the fitting range to the early stage of crystallization, where the crystallization-induced decrease in the smoothed potential energy remains smaller than approximately w.

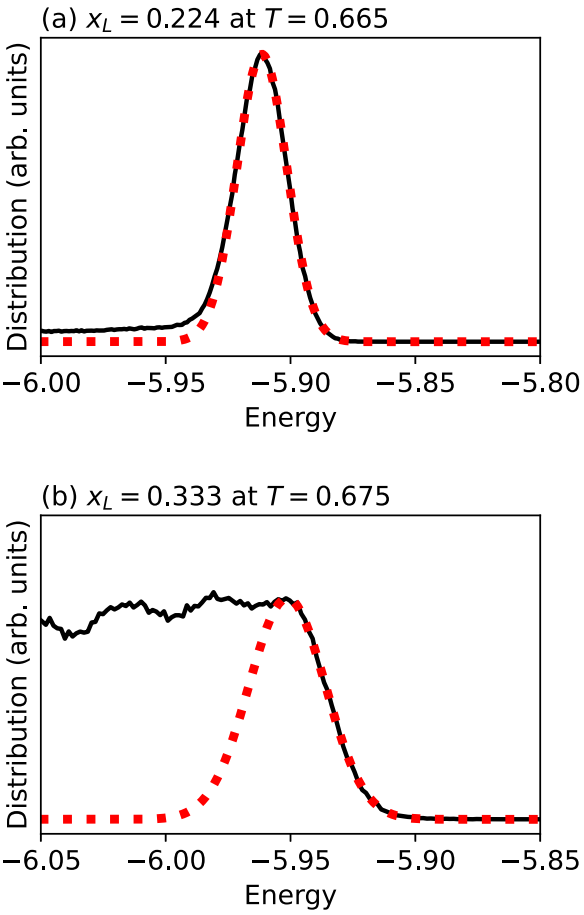


FIG. 2. Potential energy distributions $P(E)$ (solid lines) and corresponding reference Gaussians (dashed lines) for systems with (a) $x_L = 0.224$ at $T = 0.665$ and (b) $x_L = 0.333$ at $T = 0.675$.

The parameters ϵ and w are determined from a reference Gaussian constructed from the potential-energy distribution $P(E)$ obtained from 10 independent trajectories at each state point. Figure 2 illustrates two representative examples of $P(E)$. When a supercooled liquid state is formed and configurations belonging to this state are sampled sufficiently, a distinct Gaussian-like peak associated with the supercooled liquid state is expected to appear in $P(E)$. Figure 2(a) illustrates a case in which such a peak is clearly visible. By contrast, when crystallization occurs without the formation of a supercooled liquid state, a distinct Gaussian-like peak associated with the supercooled liquid state does not appear. Figure 2(b) illustrates a case in which no distinct peak is visible. Regardless of whether a supercooled liquid state is formed, $P(E)$ approaches zero at high energies and increases as E decreases from the high-energy side. When a supercooled liquid state is formed, the high-energy side of $P(E)$ is expected to be dominated by the contribution from this state. This consideration motivates us to construct a Gaussian component from the high-energy side of $P(E)$ such that, if a supercooled liquid state is formed, it corresponds to the contribution of this state to $P(E)$. We refer to such a component as the reference Gaussian. To identify the reference Gaussian,

we consider a Gaussian function centered at $E = \mu$,

$$G(E;\mu,\sigma,C) = \frac{C}{\sqrt{2\pi\sigma^2}} \exp\left(-\frac{(E-\mu)^2}{2\sigma^2}\right). \quad (4)$$

Its amplitude C and width σ are determined by fitting the function to $P(E)$ over the region $E > \mu$. Varying μ generates a family of Gaussian components, from which the reference Gaussian is selected. If a supercooled liquid state is formed, then the reference Gaussian should correspond to the contribution from this state. We therefore impose two requirements on the reference Gaussian: It should closely follow the high-energy side of $P(E)$, and it should account for a substantial portion of the high-energy side. The latter requirement is intended to exclude small Gaussian components that account for only a limited part of the high-energy side. To quantify this requirement, we introduce the quantity $A(\mu)$,

$$A(\mu) = \int_{\mu}^{\mu+2\sigma} G(E;\mu,\sigma,C)dE, \quad (5)$$

which represents the area of the Gaussian component centered at μ over the range from μ to $\mu + 2\sigma$ and thus provides a measure of how much of the high-energy side of $P(E)$ is accounted for by this component. To quantify the first requirement, we introduce the quantity $D(\mu)$,

$$D(\mu) = \int_{\mu}^{\mu+2\sigma} |P(E) - G(E;\mu,\sigma,C)|dE, \quad (6)$$

which is the integrated absolute difference between $P(E)$ and the Gaussian component centered at μ and thus provides a measure of how closely this component follows the high-energy side of $P(E)$. To balance these two requirements, we introduce the score function

$$\text{Score}(\mu) = A(\mu) - \kappa D(\mu), \quad (7)$$

where κ controls the relative penalty assigned to $D(\mu)$. Unless otherwise stated, $\kappa = 20$. We select the Gaussian component that maximizes $\text{Score}(\mu)$ as the reference Gaussian. We note that the upper limit of integration in $A(\mu)$ and $D(\mu)$ is set to $\mu + 2\sigma$, since regions beyond this point can be affected by the initial structural relaxation. This choice prevents the score from favoring small Gaussian components that account for only a limited part of the high-energy side. We then define ϵ and w as the center and width of the reference Gaussian, respectively. The fitting range is determined from ϵ and w, as described above.

Figure 2(a) shows that the Gaussian-like peak associated with the supercooled liquid state is well reproduced by the reference Gaussian. Figure 2(b) shows that, although $P(E)$ exhibits no distinct peak, its high-energy side is well reproduced by the reference Gaussian. Although this reference Gaussian does not represent a contribution from the supercooled liquid state, its center and width are used to determine the fitting range.

C. Illustrative examples

To illustrate how the lifetime is determined from the fitting procedure, Fig. 3 shows three examples of the time evolution of the potential energy for the system with $x_L = 0.224$ at different temperatures. The potential energy evolution at $T = 0.665$ is summarized in Fig. 3(a1). Using $\epsilon = -5.911$ and $w = 0.010$, the piecewise-linear fit yields $E_0 = -5.911$, $t_l = 8.68 \times 10^6$, and $\alpha = -7.99 \times 10^{-8}$. In the fitting process, Δt is determined iteratively to be 1.91×10^4, and the resulting smoothed potential-energy trajectory yields $t_{\max} = 8.80 \times 10^6$. Δt is approximately equal to $0.15(w/|\alpha|)$, satisfying the condition $0.1w/|\alpha| \leqslant \Delta t \leqslant 0.2w/|\alpha|$. The fitted parameters provide a quantitative description of the trajectory: After fluctuating around $E_0 = -5.911$, the potential energy drops sharply at $t_l = 8.68 \times 10^6$.

To confirm that the observed energy drop reflects the progression of crystallization, the corresponding time evolution of the number of loose-crystalline bipyramids per 10 000 atoms, N_{loo}, is shown in Fig. 3(a2). This quantity is evaluated every 0.1×10^6 time units. After initial fluctuations, N_{loo} increases sharply, with the onset of this increase coinciding with that of the energy drop, confirming that the observed energy drop reflects the progression of crystallization. In this analysis, crystallization is identified by the increase in N_{loo}. Ideally, however, crystallization should be identified using a structural motif that more directly reflects the underlying structural transformation. In particular, it is desirable to identify a motif whose number is nearly zero before crystallization and increases once crystallization initiates. To this end, we examine the number of loose-crystalline bipyramids with connectivity six per 10 000 atoms (N^6_{loo}). Here two bipyramids are regarded as connected if they share an apex atom, and the connectivity of a given bipyramid is defined as the number of bipyramids connected to it. For loose-crystalline bipyramids in LS_2 Laves crystals (which correspond to crystalline bipyramids), the connectivity is six [Fig. 1(i)]. Thus, the presence of connectivity-six loose-crystalline bipyramids indicates the existence of medium-range crystal-like order. Figure 3(a3) shows that N^6_{loo} remains nearly zero before t_l and increases markedly thereafter. Thus, N^6_{loo} exhibits the desired behavior for identifying crystallization onset: It remains nearly zero before crystallization and increases once crystallization initiates. While N^6_{loo} is a clear indicator of crystallization in the Wahnström alloy, a structural motif that directly captures crystallization is not always identified in other systems. In contrast, the potential energy is well defined for any system, making it more generally applicable. For this reason, in this work, we determine the lifetime based on the time evolution of the potential energy. On the other hand, since N^6_{loo} remains close to zero prior to crystallization, it enables a direct comparison of the degree of crystallinity across different temperatures and compositions. We therefore use N^6_{loo} for this purpose in Sec. V E.

Figure 3(c1) shows the time evolution of the potential energy at $T = 0.630$. Unlike Fig. 3(a1), no stationary regime is observed; instead, the energy decreases monotonically from the outset. The fitted lifetime is $t_l = 0$, indicating that crystallization occurs without the formation of a supercooled liquid state. This absence of a supercooled liquid state suggests the existence of a metastability limit. The corresponding time evolution of N^6_{loo} shows a monotonic increase from the outset [Fig. 3(c3)], indicating that the energy drop arises from crystallization rather than from the initial structural

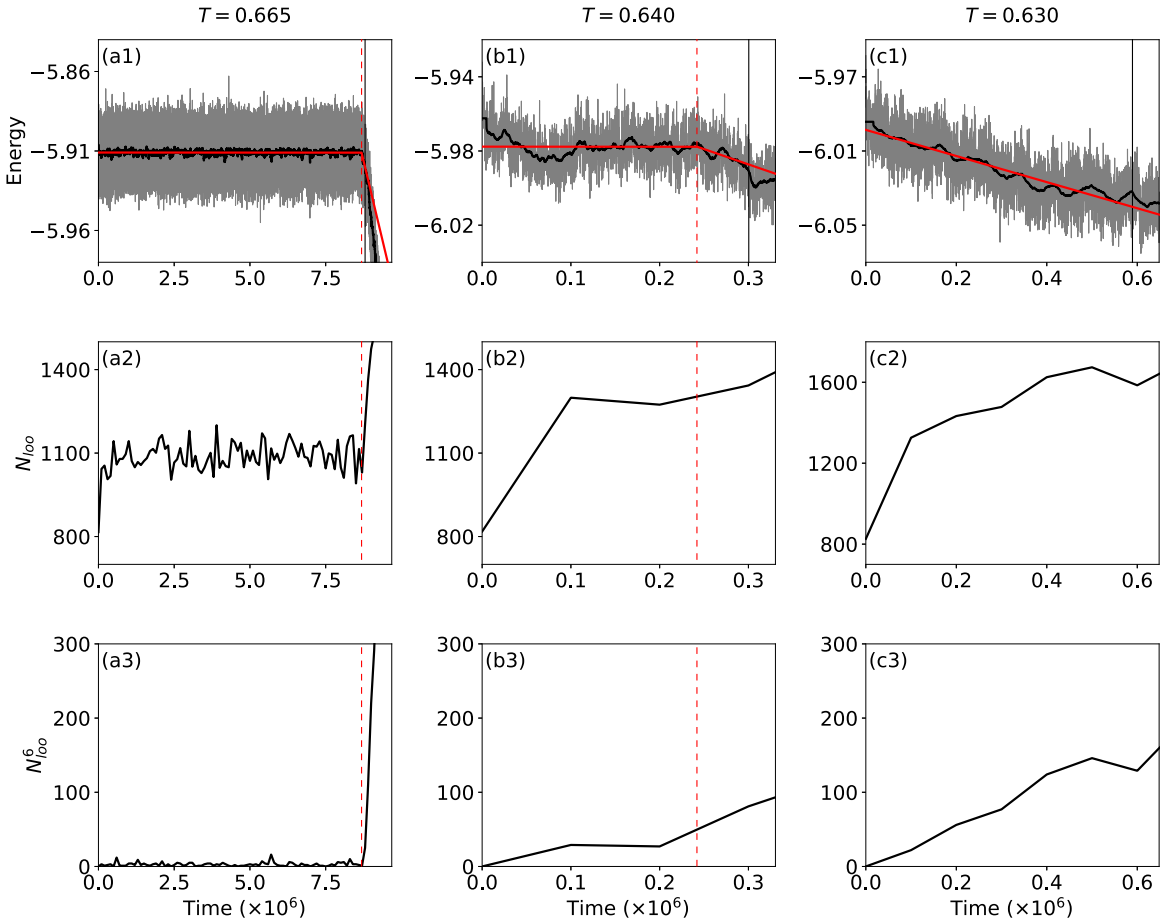


FIG. 3. Time evolution of [(a1)–(c1)] potential energy per atom, [(a2)–(c2)] number of loose-crystalline bipyramids per 10 000 atoms, and [(a3)–(c3)] number of connectivity-six loose-crystalline bipyramids per 10 000 atoms for the $x_L = 0.224$ system. Results at $T = 0.665$, 0.640, and 0.630 are shown in panels (a1)–(a3), (b1)–(b3), and (c1)–(c3), respectively. In panels (a1)–(c1), gray curves show the potential energy, black curves show the smoothed potential energy, and red lines show the fitted piecewise-linear function. Vertical solid lines indicate $t_{\max}$, the upper limit of the fitting range. Vertical dashed lines in panels (a1)–(a3) and (b1)–(b3) indicate t_l, the fitted lifetime; no vertical dashed line is shown for $T = 0.630$, for which $t_l = 0$.

relaxation following the quench. This immediate crystallization prevents the formation of the supercooled liquid state.

Care must be taken when a short but nonzero lifetime is obtained from the fitting procedure. Figure 3(b1) shows the time evolution of the potential energy at $T = 0.640$. The fitting procedure yields $t_l = 0.24 \times 10^6$. According to the present criterion, the trajectory is regarded as having formed a supercooled liquid state. Direct inspection of the energy evolution, however, does not necessarily support this conclusion. Although a nearly stationary interval is observed before crystallization, its duration is comparable to that of the preceding nonstationary regime. It is therefore unclear whether the nearly stationary interval should be regarded as a short-lived metastable equilibrium state or merely as a transient feature of an evolving system. Moreover, the fitted lifetime includes the preceding nonstationary regime. The present approach may therefore overestimate the stability of the supercooled liquid state. However, this does not weaken the evidence for the existence of a metastability limit.

V. RESULTS

A. Existence of a metastability limit

Figure 4 shows the temperature dependence of the probability that crystallization occurs without the formation of a supercooled liquid state, corresponding to a lifetime of zero. The probability at each temperature is evaluated from 10 independent MD simulations. Upon cooling, the probability increases and exceeds 50%, indicating the existence of a metastability limit. A cubic-polynomial fit to the data yields a 50% probability at $T = 0.644$. The metastability-limit temperature is therefore determined to be $T_{\rm ml} = 0.644$. Given that the liquidus temperature at $x_L = 0.224$ is $T_{\rm liq} = 0.873$ [38], $T_{\rm ml}$ corresponds to a reduced temperature of approximately 0.74 (0.644/0.873). Applying the same analysis to $x_L = 0.333$ and 0.520 shows that these systems also exhibit a metastability limit, with $T_{\rm ml} = 0.693$ and 0.676, respectively. These values correspond to approximately 78% and 80% of the respective liquidus temperatures. The metastability-limit temperatures are summarized in Table I. Our results show

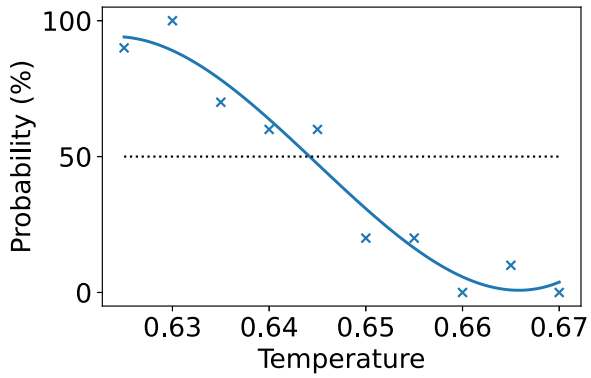


FIG. 4. Temperature dependence of the probability that the lifetime is zero for the system with $x_L = 0.224$. The solid curve shows a cubic-polynomial fit to the data. The horizontal dashed line indicates a probability of 50%.

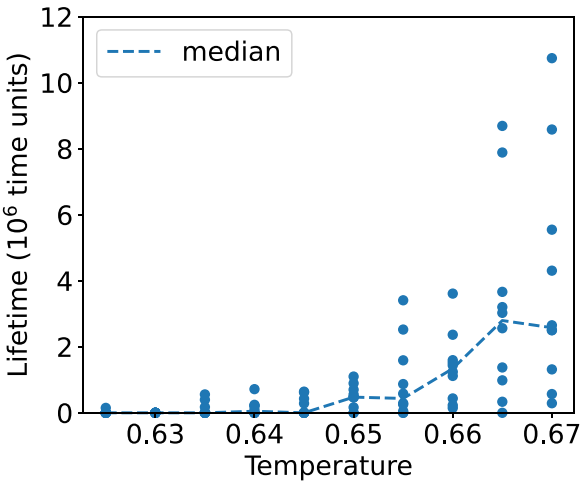


FIG. 5. Temperature dependence of the lifetime of the supercooled liquid state for the system with $x_L = 0.224$. Filled circles represent lifetimes obtained from 10 independent simulations at each temperature. The dashed line is a guide to the eye connecting the median lifetimes.

that a metastability limit exists for compositions between the two eutectic points at $x_L = 0.224$ and $x_L = 0.520$ and that $T_{\rm ml}$ depends on composition. Here $x_L = 0.224$ corresponds to the eutectic point between the S-atom fcc and LS_2 phases, and $x_L = 0.520$ corresponds to that between the L-atom fcc and LS_2 phases. Rapid crystallization in the Wahnström alloy has previously been reported in molecular dynamics simulations [27,28]. The present results suggest that the reported behavior may be a manifestation of a metastability limit, although this interpretation was not discussed in the previous studies.

Note that, although the value of $T_{\rm ml}$ depends slightly on the control parameters λ and κ, the existence of a metastability limit remains unchanged. For example, for the system with $x_L = 0.224$, $T_{\rm ml} = 0.644$, 0.636, 0.643, and 0.635 for $(\lambda, \kappa) = (1, 20)$, (2,20), (1,10), and (2,10), respectively.

The results presented above were obtained using an instantaneous quench from the liquidus temperature. To examine whether the cooling protocol affects the existence of a metastability limit, we performed additional simulations in which the systems were cooled gradually to the target temperature and subsequently annealed. For each composition, we chose a cooling rate as low as possible while avoiding crystallization during cooling. The cooling rates used were $q = 10^{-5}$, 10^{-5}, and 10^{-6} for $x_L = 0.224$, 0.333, and 0.520, respectively. Crystallization did not occur during cooling at these rates, as discussed in Sec. V E. The systems were cooled to $T = 0.625$, 0.665, and 0.655, respectively, and then annealed at these temperatures. Four independent simulations were performed for each condition. For $x_L = 0.333$ and 0.520, no trajectory formed a supercooled liquid state. For $x_L = 0.224$, two of the four trajectories formed a supercooled liquid state, although the resulting lifetimes were short. To improve the statistics for $x_L = 0.224$, 10 additional independent simulations were carried out under the same conditions. Among these 10 trajectories, only two formed a supercooled liquid state. These results indicate that the existence of the metastability limit is not a consequence of the instantaneous temperature quench employed in the preceding simulations.

A detailed analysis of the finite lifetime is not essential for identifying the metastability limit. Nevertheless, for completeness, we briefly present the temperature dependence of the lifetime of the supercooled liquid state below. Figure 5 shows the individual lifetimes and their median as a function of temperature for the system with $x_L = 0.224$. Although the individual lifetimes exhibit noticeable scatter at high temperatures, the median lifetime shows an overall decrease with decreasing temperature. Figure 6 compares the temperature dependence of the median lifetime of the supercooled liquid state for $x_L = 0.224$, 0.333, and 0.520.

TABLE I. Liquidus temperature ($T_{\rm liq}$), metastability-limit temperature ($T_{\rm ml}$), and onset temperatures (T_o) at $q = 10^{-8}$ and $q = 10^{-7}$ for systems with $x_L = 0.224$, 0.333, and 0.520.

x_L	0.224	0.333	0.520
$T_{\rm liq}$	0.873	0.886	0.847
$T_{\rm ml}$	0.644	0.693	0.676
T_o at $q = 10^{-8}$	0.656	0.703	0.679
T_o at $q = 10^{-7}$		0.686	

B. Immediate systemwide local crystallization

In this section, we further examine how crystallization proceeds below $T_{\rm ml}$ by performing additional simulations of systems containing 100 000 atoms. The larger system size allows us to analyze the spatial distribution of crystalline domains. Here a crystalline domain is defined as a supercluster composed of connectivity-six loose-crystalline bipyramids and the loose-crystalline bipyramids connected to them.

Equilibrated liquids at their respective liquidus temperatures are instantaneously quenched to $T = 0.600$, and the subsequent time evolution of the system is analyzed. Because similar behavior is observed for $x_L = 0.224$, 0.333, and 0.520, we present the results for $x_L = 0.224$ as a representative example. Figure 7(a) shows that the potential energy decreases monotonically from the outset, apart from fluctuations, indicating that crystallization initiates immediately after the

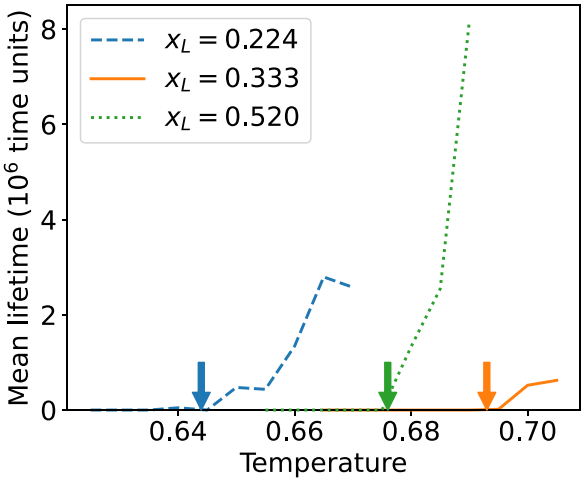


FIG. 6. Temperature dependence of the median lifetime of the supercooled liquid state at $x_L = 0.224$, 0.333, and 0.520. Arrows indicate the estimated metastability-limit temperatures.

quench without the formation of a supercooled liquid state. Figure 7(b) shows the corresponding time evolution of N_{loo}^6, the number of connectivity-six loose-crystalline bipyramids. The increase in N_{loo}^6 from the outset confirms the immediate onset of crystallization. Figure 8 illustrates the time evolution

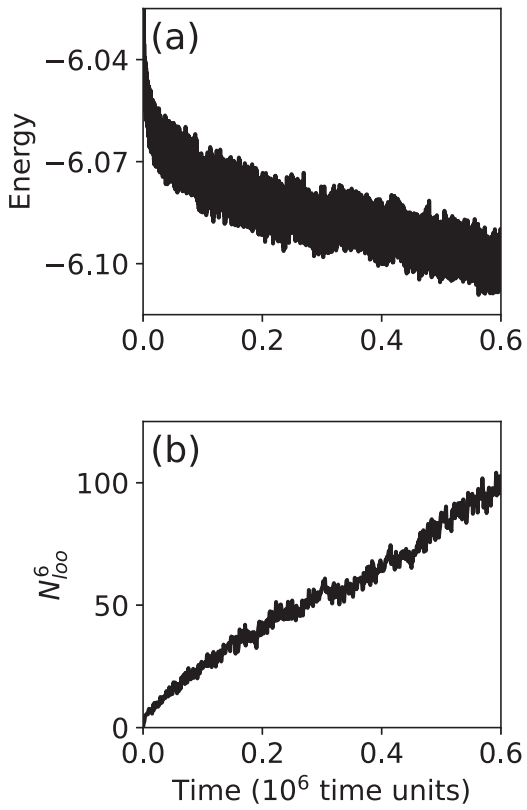


FIG. 7. Time evolution for the system with $x_L = 0.224$ composed of 100 000 atoms at $T = 0.600$: (a) The potential energy per atom evaluated every 1 time units and (b) the number of connectivity-six loose-crystalline bipyramids per 10 000 atoms (N_{loo}^6) evaluated every 0.001×10^6 time units.

of the spatial distribution of crystalline domains, indicating that local crystalline domains form throughout the system.

To provide a more detailed view of the dynamics, a movie is available as Supplemental Material [43]. It shows that crystalline domains repeatedly emerge and disappear throughout the system during the early stage, while the overall number of crystalline domains increases with time. As time proceeds, long-lived domains emerge at spatially separated locations and subsequently grow, suggesting that crystallization occurs simultaneously in different regions of the system. Figure 9(a) shows the domain size S (the number of atoms in a domain) as a function of rank, where the domains are ranked in descending order of S. Representative results at $t = 0.000$, 0.050, and 0.600 are shown. The number of crystalline domains (N_{dom}) and the size of the rank-1 domain (S_1) obtained from the rank-size analysis are shown as functions of time in Figs. 9(b) and 9(c), respectively. At $t = 0$, only two crystalline domains are present. N_{dom} rapidly increases to 90 by $t = 0.050$, confirming immediate crystallization. Together with the spatial distributions shown in Fig. 8, the rapid increase in N_{dom} indicates that local crystallization initiates immediately throughout the system. Similar behavior has been reported for Ni and Al [11,44]. Figure 9(c) shows that S_1 increases rapidly after $t \approx 0.5$. However, the movie does not show any corresponding acceleration in the growth of a single domain. This suggests that the increase in S_1 arises from the merging of previously separate crystalline domains. Figure 8 further shows that many connectivity-six loose-crystalline bipyramids are part of pentagonal rings. Since pentagonal rings are characteristic of fivefold twins [24], this observation supports previous findings that fivefold twinlike motifs are involved in the onset of crystallization [29].

Glassy materials often contain nanoscale crystalline regions [45], whose presence can enhance their physical properties [46–49]. Our results suggest that crystallization occurring below T_{ml} may contribute to the formation of such nanoscale crystalline regions. These findings imply that controlling crystallization below T_{ml} may provide a route to tuning the properties of glassy materials.

C. System-size dependence of metastability

For a supercooled liquid just below the liquidus temperature, the critical nucleus size for crystallization is extremely large but finite. As the system size increases, the probability of finding such a growing crystalline nucleus somewhere in the system approaches unity [4], implying that crystallization has already started in the system. Therefore, in the thermodynamic limit, the supercooled liquid state—defined here as a metastable equilibrium state—is not expected to exist.

This argument suggests that the metastability-limit temperature should exhibit a system-size dependence. To examine this possibility, we quantitatively evaluate the system-size dependence of both the lifetime and the metastability-limit temperature. Such an analysis requires a large number of independent crystallization trajectories. We therefore consider systems composed only of L atoms rather than the binary mixtures studied above. Because crystallization occurs more readily in the pure system, independent crystallization trajectories can be collected efficiently. Simulations were per-

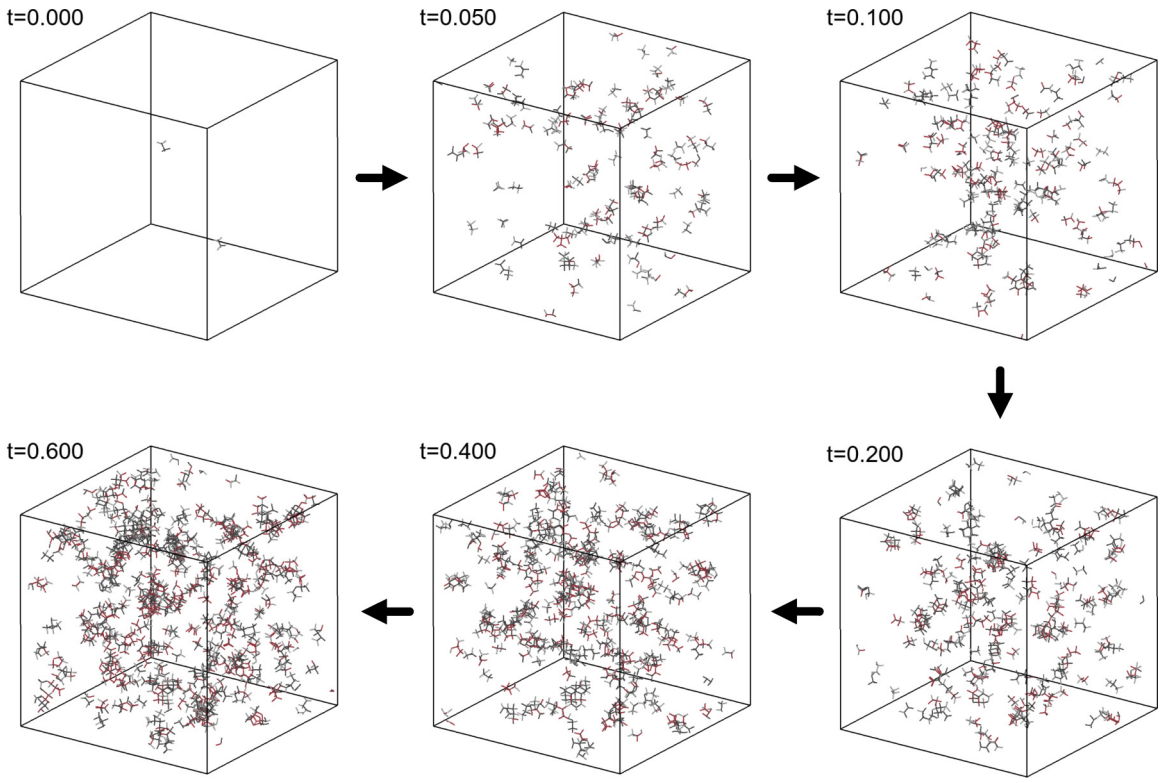


FIG. 8. Time evolution of the spatial distribution of crystalline domains. For clarity, only the apex bonds of connectivity-six loose-crystalline bipyramids are shown. Bonds forming complete or partial pentagonal rings are highlighted in red.

formed for systems containing $N = 10^4$, $(10/3) \times 10^4$, and 10^5 atoms. At each temperature, 1000 independent trajectories were generated. To estimate statistical uncertainties, the trajectories were divided into two equal groups, and the standard deviations of the resulting estimates were used as measures of the statistical uncertainties. For the pure system, once crystallization initiates, it proceeds rapidly. Consequently, the initial structural relaxation regime occupies a substantial fraction of the fitting range. Since the piecewise-linear model does not account for the initial relaxation, this model frequently fails to reproduce the overall shape of the potential-energy curve. To minimize the effect of the initial structural relaxation process, the systems were cooled gradually to the target temperature at a rate of $q = 5 \times 10^{-2}$. During cooling, the thermostat and barostat damping constants were set to 0.005 and 1.0, respectively. After the target temperature was reached, they were set to 0.1 and 1.0, respectively. Although this cooling protocol does not completely eliminate cooling-induced structural relaxation, the overall shape of the potential-energy curve can be reasonably reproduced by the piecewise-linear model. Further reduction of the cooling rate can lead to crystallization during cooling before the lifetime measurement begins, thereby preventing a reliable determination of the lifetime. In addition, the fitting-range parameter was set to $\lambda = 4$ rather than $\lambda = 1$, because the latter occasionally failed to detect the formation of a supercooled liquid state in the pure system. Figure 10(a) shows that the metastability-limit temperature shifts to higher temperatures as N increases. The estimated metastability-limit temperatures are $T_{\mathrm{ml}} = 0.869$, 0.899, and 0.916 for $N = 10^4$, $(10/3) \times 10^4$, and 10^5, respectively, with statistical uncertainties smaller than 0.001. This behavior is accompanied by a systematic decrease in the lifetime at a fixed temperature with increasing system size [Fig. 10(b)].

D. Interpretation of the metastability limit

The observed increase in T_{ml} with system size is consistent with the argument presented above. This trend suggests that T_{ml} approaches the liquidus temperature as the system size increases and that the supercooled liquid state (defined as a metastable equilibrium state) ceases to exist in the thermodynamic limit. This raises a fundamental question: If the supercooled liquid state does not exist in the thermodynamic limit, then what is the physical significance of the supercooled liquid state and the associated metastability limit identified in finite systems?

To address this question, let $T_{\mathrm{ml}}(N)$ denote the metastability-limit temperature for a system containing N atoms. For larger systems, the corresponding $T_{\mathrm{ml}}(N)$ is expected to shift to higher temperatures. In the limit $N \to \infty$, it approaches the liquidus temperature. From this perspective, $T_{\mathrm{ml}}(N)$ may be regarded as a lower estimate of the metastability-limit temperature in a macroscopic system.

While this interpretation is useful, it does not fully capture the physical significance of $T_{\mathrm{ml}}(N)$. A more intrinsic understanding emerges by reinterpreting $T_{\mathrm{ml}}(N)$ in terms of the lifetime of liquidlike regions of size N in a macroscopic system. To clarify this viewpoint, let $t_l(N, T)$ denote the lifetime of the supercooled liquid state for a microscopic system of size N at temperature T. Consider a liquidlike region of size N in a macroscopic system, initially free of any growing crystalline domains. If the effects of periodic boundary

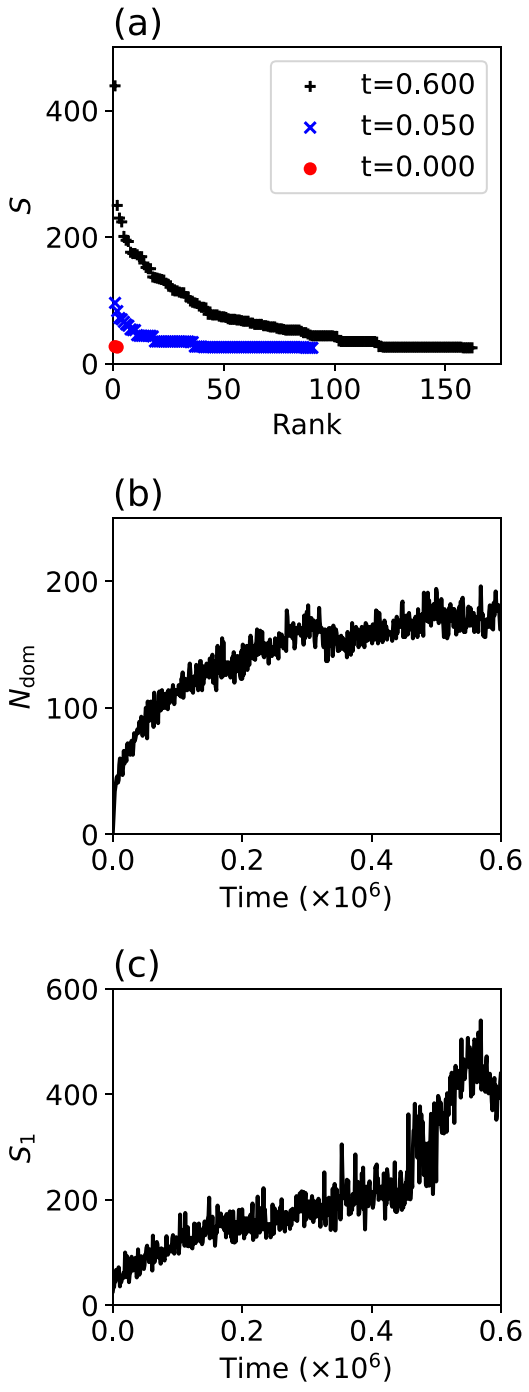


FIG. 9. Time evolution for the system with $x_L = 0.224$ composed of 100 000 atoms at $T = 0.600$: (a) The domain size S (the number of atoms in a domain) as a function of rank, where the domains are ranked in descending order of size, at $t = 0.000$, 0.050, and 0.600; (b) the number of crystalline domains per 100 000 atoms (N_{dom}); and (c) the size of the rank-1 crystalline domain (S_1). Panels (b) and (c) are evaluated every 0.001×10^6 time units.

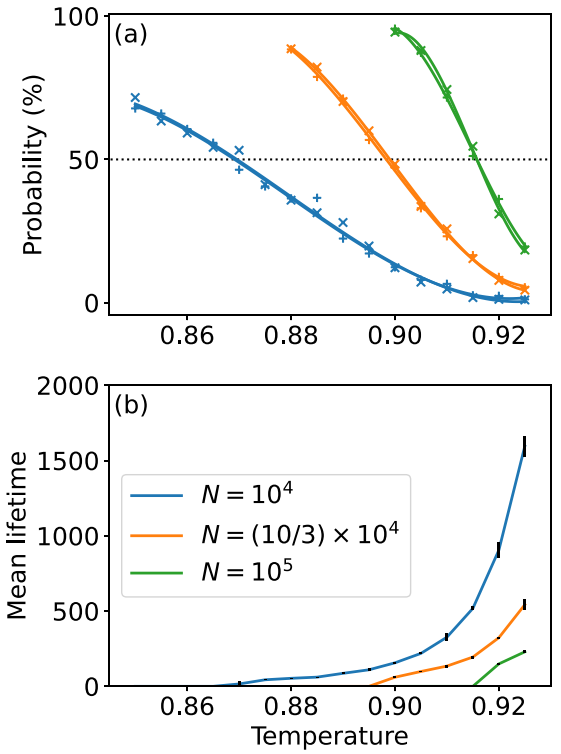


FIG. 10. System-size dependence of the stability of the supercooled liquid state in the pure L-atom system. (a) Temperature dependence of the probability that the system crystallizes without forming a supercooled liquid state. Blue, orange, and green data correspond to $N = 10^4$, $(10/3) \times 10^4$, and 10^5, respectively. The + and × symbols represent estimates obtained from two independent groups of 500 trajectories. Solid lines are cubic fits to the data. The horizontal dashed line indicates a probability of 50%. (b) Median lifetime of the supercooled liquid state as a function of temperature. Colors are the same as in panel (a). Error bars indicate the standard deviations estimated from the two independent groups and are mostly comparable to the line width at low temperatures.

conditions can be neglected, then the quantity $t_l(N, T)$ provides an estimate of the timescale over which such a region remains in a liquidlike state at temperature T. Since larger regions tend to have shorter lifetimes, $T_{\mathrm{ml}}(N)$ can be interpreted as the temperature below which liquidlike regions larger than N in a macroscopic system cannot exist as metastable states.

E. Metastability limit and the competition between glass formation and crystallization during cooling

The temperature dependence of N_{loo}^6, the number of connectivity-six loose-crystalline bipyramids, during cooling from the liquidus temperature at different rates q is shown in Fig. 11(a1)–11(c1) for the systems with $x_L = 0.224$, 0.333, and 0.520. The corresponding cooling-rate dependence of N_{loo}^6 at the final temperature ($T = 0.500$) is shown in Figs. 11(a2)–11(c2). At high temperatures, N_{loo}^6 remains negligibly small regardless of q. For relatively high cooling rates, it exhibits little variation during cooling, indicating that crystallization is suppressed and the system forms a glass. Consistent with this behavior, N_{loo}^6 at $T = 0.500$ remains close to zero down to $q = 10^{-5}$ for $x_L = 0.224$ and 0.333 and down to $q = 10^{-6}$ for $x_L = 0.520$. Furthermore, the corresponding $g(r)$ curves at $T = 0.500$ remain typical of amorphous structures. Unlike the $q = 10^{-8}$ samples, which exhibit a discernible substructure within the second peak of $g(r)$ indicative of enhanced

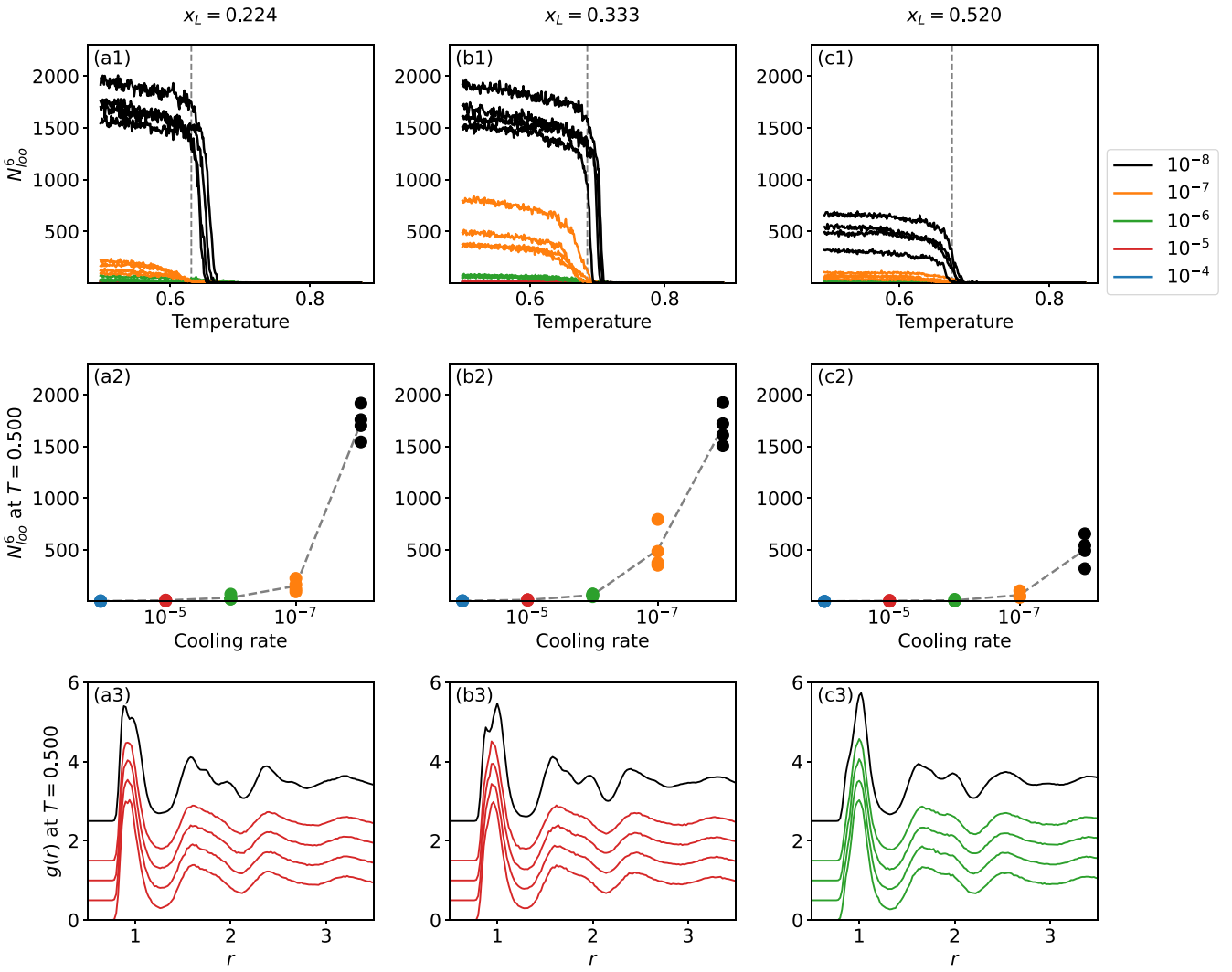


FIG. 11. Development of crystalline order during cooling. [(a1)–(c1)] Temperature dependence of the number of connectivity-six loose-crystalline bipyramids per 10 000 atoms during cooling at different rates. [(a2)–(c2)] Cooling-rate dependence of the number at the final temperature $T = 0.500$. [(a3)–(c3)] Radial distribution functions $g(r)$ at the final temperature $T = 0.500$. Panels (a1)–(a3), (b1)–(b3), and (c1)–(c3) correspond to $x_L = 0.224$, 0.333, and 0.520, respectively. Individual results from four independent simulations are shown for each cooling rate in (a1)–(c1) and (a2)–(c2). In (a3)–(c3), the upper curves show averages over four independent simulations cooled at $q = 10^{-8}$, whereas the lower curves show individual simulations cooled at $q = 10^{-5}$ for $x_L = 0.224$ and 0.333 and at $q = 10^{-6}$ for $x_L = 0.520$. The vertical dashed lines in (a1)–(c1) indicate the estimated metastability-limit temperatures. The vertical dashed lines in (a2)–(c2) are guides to the eye connecting the average values.

crystalline ordering, no such features are observed at $q = 10^{-5}$ for $x_L = 0.224$ and 0.333 and at $q = 10^{-6}$ for $x_L = 0.520$. These observations provide additional evidence that crystallization is suppressed and the systems remain glassy at these cooling rates. The absence of detectable crystallization places an upper bound on the critical cooling rate. For $x_L = 0.224$ and 0.333, a small but visible increase in N^6_{loo} is observed when the cooling rate is reduced from 10^{-5} to 10^{-6}. Similarly, for $x_L = 0.520$, a visible increase appears when the cooling rate is reduced from 10^{-6} to 10^{-7}. These observations place the critical cooling rate between 10^{-5} and 10^{-6} for $x_L = 0.224$ and 0.333, and between 10^{-6} and 10^{-7} for $x_L = 0.520$. Based on these results, we selected cooling rates of $q = 10^{-5}$ for $x_L = 0.224$ and $x_L = 0.333$ and $q = 10^{-6}$ for $x_L = 0.520$ for the gradual-cooling stage preceding the lifetime measurements described in Sec. V A. Below the metastability-limit temperature T_{ml}, crystallization is expected to initiate immediately. However, even in this regime, no significant increase in N^6_{loo} is observed at high cooling rates. This is because crystal growth requires a finite time, and the system is rapidly cooled to lower temperatures before crystalline regions can grow to a detectable size.

As q is reduced to values just below the critical cooling rate, a sharp rise in N^6_{loo} over a narrow temperature range becomes visible during cooling, providing a clear signature of the onset of crystallization. The final value of N^6_{loo} at $T = 0.500$ also increases noticeably. For $x_L = 0.224$, a well-developed sharp rise is observed at $q = 10^{-8}$, whereas at $q = 10^{-7}$ only a gradual increase is seen, with no identifiable sharp rise. For $x_L = 0.333$, a sharp rise is observed at both $q = 10^{-7}$

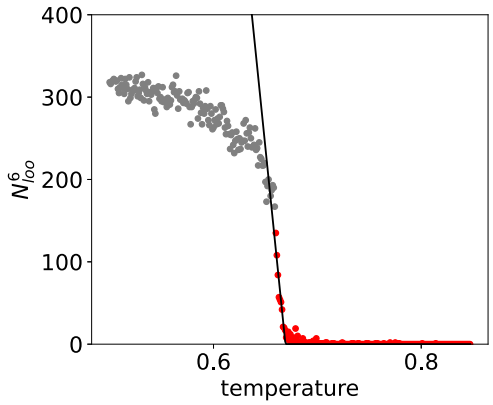


FIG. 12. Determination of the onset temperature of crystallization. Circles represent the temperature dependence of N^6_{loo} for the system with $x_L = 0.520$ during cooling at $q = 10^{-8}$. Red circles indicate the data used for the fit. The fitted onset temperature is $T_o = 0.669$.

and $q = 10^{-8}$, with the latter showing a well-developed one. For $x_L = 0.520$, a sharp rise is also observed at $q = 10^{-8}$, although it is not yet well developed.

We refer to the temperature at which N^6_{loo} exhibits a sharp rise as the onset temperature of crystallization (T_o). To determine T_o for each trajectory, we fit the T–N^6_{loo} curve to a piecewise-linear function,

$$N(T) = \begin{cases} \beta(T - T_o) & T < T_o, \\ 0 & T \geqslant T_o. \end{cases} \tag{8}$$

Here $\beta < 0$, so that $N(T)$ increases with decreasing temperature, reflecting the increase in N^6_{loo} as crystallization proceeds. We fit the data in the temperature range where N^6_{loo} remains below half of its value at $T = 0.500$. The fitted parameter T_o is then taken as the onset temperature for the trajectory. As an example, Fig. 12 illustrates the determination of T_o for a trajectory with $x_L = 0.520$ at $q = 10^{-8}$. For each value of q, the onset temperature T_o is defined as the average over four independent trajectories.

For $x_L = 0.224$ at $q = 10^{-8}$, the onset temperature is $T_o = 0.656 \pm 0.006$. Here the uncertainty represents the standard deviation over independent trajectories. The onset temperature is close to the metastability-limit temperature $T_{\mathrm{ml}} = 0.644$ and far below the liquidus temperature $T_{\mathrm{liq}} = 0.873$. These results indicate that, during cooling at rates close to the critical cooling rate, crystallization initiates near T_{ml}. The same behavior is also observed for $x_L = 0.333$ and 0.520. The onset temperatures are summarized in Table I.

To place the onset temperature in a broader context, we consider more general systems. Even in systems that do not exhibit a metastability limit, a sharp rise in the T-crystallinity curve is expected to emerge as q decreases, allowing T_o to be identified at cooling rates close to the critical cooling rate. However, in such systems, T_o is unrelated to T_{ml}. Even when a metastability limit exists, the evolution of the T-crystallinity curve with decreasing q depends on both the temperature dependence of the lifetime and that of the crystal growth rate. Therefore, T_o does not necessarily lie near T_{ml}. However, if (i) the lifetime of the supercooled liquid increases sharply above T_{ml} and (ii) the temperature at which the crystal growth rate is maximized is not significantly lower than T_{ml}, then T_o determined at cooling rates close to the critical cooling rate is expected to lie near T_{ml}.

Our results also provide insight into the composition dependence of glass-forming ability. Although the critical cooling rate is commonly used as a quantitative measure of glass-forming ability, its precise value is not determined in this study. Therefore, we compare the crystallization behavior at a fixed cooling rate $q = 10^{-7}$. A sharp rise in N^6_{loo} is observed at $x_L = 0.333$, whereas no sharp rise is observed at $x_L = 0.224$ and 0.520. This indicates that crystallization occurs more readily at the stoichiometric composition ($x_L = 0.333$), whereas it is suppressed at the nonstoichiometric compositions ($x_L = 0.224$ and 0.520). These results suggest that the nonstoichiometric systems exhibit higher glass-forming ability than the stoichiometric system.

VI. A CONCEPTUAL PERSPECTIVE ON THE DEFINITION OF GLASS

The question of what constitutes a glass has long been a subject of debate [13–16], and a universally accepted definition remains elusive. In this work, we use the term "glass" to denote noncrystalline solidlike materials with liquidlike disordered structures. This usage is adopted only for practical convenience and is not intended to advocate any particular definition of glass.

One might regard the question "What is a glass?" as merely a matter of terminology. However, choosing a useful definition is closely related to finding a meaningful way to classify states of matter, and the search for such a classification can contribute to progress in our understanding of the underlying physics. The presence or absence of a metastability limit provides a physically meaningful criterion for characterizing the behavior of a system. This criterion is conceptually independent of how the term "glass" is defined: It may be incorporated into a definition of glass, but it can also be used separately. It is therefore meaningful to discuss the implications of a metastability limit for defining glass.

One viewpoint proposed in the literature interprets a glass as a nonequilibrium state evolving toward a supercooled liquid state [14]. Within this viewpoint, the existence of a supercooled liquid state is an essential prerequisite. If the system exhibits a metastability limit, then below T_{ml} there is no supercooled liquid state toward which the system can evolve. It follows that, within this viewpoint, noncrystalline states below T_{ml} do not qualify as glasses. We also note that, as discussed in Sec. V D, in systems exhibiting a metastability limit, no supercooled liquid state exists in the thermodynamic limit, and therefore the notion of a supercooled liquid state may be meaningful only in a local sense. In approaches that define glass through its relation to a supercooled liquid state, the notion of glass may likewise be meaningful only in a local sense.

VII. CONCLUSION

To gain insight into the nature of the metastability limit, including whether it is universal or material-specific, we have investigated the metastability limit in the Wahnström alloy, a

model Laves-phase-forming system. Our molecular dynamics simulations, together with p_3 structural analysis, show that this alloy exhibits a metastability limit, characterized by a composition-dependent metastability-limit temperature T_{ml}. In isothermal annealing below T_{ml}, local crystalline domains form immediately after the quench throughout the system. Given that the formation of nanoscale crystalline regions has been reported to enhance the physical properties of glassy materials, our results suggest that controlling crystallization below T_{ml} may offer a route to tuning these properties. During cooling at rates close to the critical cooling rate, crystallization initiates near T_{ml}. This indicates that the metastability limit influences the competition between glass formation and crystallization. Furthermore, consideration of the system-size dependence of metastability suggests that the value of T_{ml} for a microscopic system provides a measure of the stability of liquidlike regions in a macroscopic system. Below T_{ml}, liquidlike regions in a macroscopic system are unlikely to exist as metastable equilibrium states if their size exceeds that of the microscopic system from which T_{ml} is determined. We have also discussed the implications of a metastability limit for defining glass. One viewpoint proposed in the literature interprets a glass as a nonequilibrium state evolving toward a supercooled liquid state. Within this viewpoint, noncrystalline states below T_{ml} do not qualify as glasses. More broadly, because no supercooled liquid state exists in the thermodynamic limit, the notion of a supercooled liquid state may be meaningful only in a local sense. This suggests that the notion of glass may likewise be meaningful only in a local sense when glass is defined through its relation to a supercooled liquid state. The existence of a metastability limit was originally proposed as a possible resolution of the Kauzmann paradox. Our findings show that its significance extends beyond this context, with implications for glass formation, the control of material properties via structural design, and the definition of glass.

ACKNOWLEDGMENTS

This work was supported by JSPS KAKENHI (Grant No. 23K03351), as well as by the computer resources provided by the Research Institute for Information Technology, Kyushu University (General Projects), and the Information Technology Center, The University of Tokyo (Wisteria/BDEC-01).

DATA AVAILABILITY

The data that support the findings of this article are openly available [50].

[1] D. Turnbull and R. E. Cech, Microscopic observation of the solidification of small metal droplets, J. Appl. Phys. **21**, 804 (1950).
[2] F. C. Frank, Supercooling of liquids, Proc. R. Soc. Lond. A **215**, 43 (1952).
[3] P. G. Debenedetti, *Metastable Liquids* (Princeton University Press, Princeton, NJ, 1996).
[4] A. Cavagna, Supercooled liquids for pedestrians, Phys. Rep. **476**, 51 (2009).
[5] H. Tanaka, Possible resolution of the Kauzmann paradox in supercooled liquids, Phys. Rev. E **68**, 011505 (2003).
[6] A. Cavagna, A. Attanasi, and J. Lorenzana, Viscoelasticity and metastability limit in supercooled liquids, Phys. Rev. Lett. **95**, 115702 (2005).
[7] E. D. Zanotto and D. R. Cassar, The race within supercooled liquids—Relaxation versus crystallization, J. Chem. Phys. **149**, 024503 (2018).
[8] A. Cavagna, I. Giardina, and T. S. Grigera, Glass and polycrystal states in a lattice spin model, J. Chem. Phys. **118**, 6974 (2003).
[9] I. Saika-Voivod, R. K. Bowles, and P. H. Poole, Crystal nucleation in a supercooled liquid with glassy dynamics, Phys. Rev. Lett. **103**, 225701 (2009).
[10] F. Trudu, D. Donadio, and M. Parrinello, Freezing of a Lennard-Jones fluid: From nucleation to spinodal regime, Phys. Rev. Lett. **97**, 105701 (2006).
[11] Y. Li, Z. Liu, P. Peng, and K. Dong, Spinodal limits of supercooled liquid Al deduced from configuration heredity of crystal clusters, Comput. Mater. Sci. **207**, 111316 (2022).
[12] W. Kauzmann, The nature of the glassy state and the behavior of liquids at low temperatures., Chem. Rev. **43**, 219 (1948).
[13] P. K. Gupta, Non-crystalline solids: Glasses and amorphous solids, J. Non-Cryst. Solids **195**, 158 (1996).
[14] E. D. Zanotto and J. C. Mauro, The glassy state of matter: Its definition and ultimate fate, J. Non-Cryst. Solids **471**, 490 (2017).
[15] J. W. P. Schmelzer and T. V. Tropin, Glass transition, crystallization of glass-forming melts, and entropy, Entropy **20**, 103 (2018).
[16] G. Benjamin, T. Gilles, and B. Ludovic, Is glass a state of matter? Phys. Chem. Glasses: Eur. J. Glass Sci. Technol. B **63**, 136 (2022).
[17] C. A. Angell and J. Donnella, Mechanical collapse vs ideal glass formation in slowly vitrified solutions: A plausibility test, J. Chem. Phys. **67**, 4560 (1977).
[18] F. Yonezawa, Glass transition and relaxation of disordered structures Solid State Phys. **45**, 179 (1991).
[19] W. Kob and H. C. Andersen, Testing mode-coupling theory for a supercooled binary Lennard-Jones mixture I: The van Hove correlation function, Phys. Rev. E **51**, 4626 (1995).
[20] D. Coslovich and G. Pastore, Understanding fragility in supercooled Lennard-Jones mixtures. I. Locally preferred structures, J. Chem. Phys. **127**, 124504 (2007).
[21] U. R. Pedersen, T. B. Schrøder, J. C. Dyre, and P. Harrowell, Geometry of slow structural fluctuations in a supercooled binary alloy, Phys. Rev. Lett. **104**, 105701 (2010).
[22] U. R. Pedersen, I. Douglass, and P. Harrowell, How a supercooled liquid borrows structure from the crystal, J. Chem. Phys. **154**, 054503 (2021).
[23] K. Nishio, A. K. A. Lu, and T. Miyazaki, Entropy-driven docosahedral short-range order in simple liquids and glasses, Phys. Rev. E **99**, 022121 (2019).

[24] K. Nishio and A. K. A. Lu, Unveiling a medium-range structural commonality of amorphous alloys, J. Non-Cryst. Solids **624**, 122696 (2024).
[25] D. Coslovich, L. Galliano, and L. Costigliola, Freezing, melting, and the onset of glassiness in binary mixtures, J. Chem. Phys. **162**, 061102 (2025).
[26] F. Leoni, J. Russo, F. Sciortino, and T. Yanagishima, Generating ultrastable glasses by homogenizing the local virial stress, Phys. Rev. Lett. **134**, 128201 (2025).
[27] U. R. Pedersen, N. P. Bailey, J. C. Dyre, and T. B. Schrøder, Crystallization of the Wahnström binary Lennard-Jones liquid arXiv:0706.0813.
[28] Z. Wang, B. Riechers, P. M. Derlet, and R. Maaß, Atomic cluster dynamics causes intermittent aging of metallic glasses, Acta Mater. **267**, 119730 (2024).
[29] K. Nishio, Effect of liquid structure on kinetic stability and glassy motifs, Phys. Rev. E **113**, 055419 (2026).
[30] G. Wahnström, Molecular-dynamics study of a supercooled two-component Lennard-Jones system, Phys. Rev. A **44**, 3752 (1991).
[31] F. Stein and A. Leineweber, Laves phases: A review of their functional and structural applications and an improved fundamental understanding of stability and properties, J. Mater. Sci. **56**, 5321 (2021).
[32] D. Wang, T. Dasgupta, van der Wee, E.B., *et al.*, Binary icosahedral clusters of hard spheres in spherical confinement, Nat. Phys. **17**, 128 (2021).
[33] K. Nishio and T. Miyazaki, How to describe disordered structures, Sci. Rep. **6**, 23455 (2016).
[34] K. Nishio and T. Miyazaki, Notation for chemical arrangements in alloys, Phys. Rev. Res. **2**, 023193 (2020).
[35] K. Nishio, Vorotis: Software for Voronoi tessellation analysis using the polyhedron code, Comput. Phys. Commun. **278**, 108418 (2022).
[36] K. Nishio, Cluster classification by chemi-topology, Comput. Phys. Commun. **286**, 108659 (2023).
[37] K. Nishio, LCS: A post-processing tool for analyzing loose-crystalline superclusters (Version 1.1.0) [Computer software], Zenodo, 2026, https://doi.org/10.5281/zenodo.24074232.
[38] K. Nishio, Liquidus curve of a Lennard-Jones mixture, Phys. Rev. E **109**, 044110 (2024).
[39] A. P. Thompson, H. M. Aktulga, R. Berger, D. S. Bolintineanu, W. M. Brown, P. S. Crozier, P. J. in 't Veld, A. Kohlmeyer, S. G. Moore, T. D. Nguyen *et al.*, LAMMPS—A flexible simulation tool for particle-based materials modeling at the atomic, meso, and continuum scales, Comput. Phys. Commun. **271**, 108171 (2022).
[40] W. Shinoda, M. Shiga, and M. Mikami, Rapid estimation of elastic constants by molecular dynamics simulation under constant stress, Phys. Rev. B **69**, 134103 (2004).
[41] F. C. Frank and J. S. Kasper, Complex alloy structures regarded as sphere packings. I. Definitions and basic principles, Acta Crystallogr. **11**, 184 (1958).
[42] J. D. Honeycutt and H. C. Andersen, Molecular dynamics study of melting and freezing of small Lennard-Jones clusters, J. Phys. Chem. **91**, 4950 (1987).
[43] See Supplemental Material at http://link.aps.org/supplemental/10.1103/wh25-ltlc for a more detailed view of the dynamics.
[44] D. V. Louzguine-Luzgin, M. Miyama, K. Nishio, A. A. Tsarkov, and A. L. Greer, Vitrification and nanocrystallization of pure liquid Ni studied using molecular-dynamics simulation, J. Chem. Phys. **151**, 124502 (2019).
[45] A. Hirata, Y. Hirotsu, T. Ohkubo, T. Hanada, and V. Z. Bengus, Compositional dependence of local atomic structures in amorphous $Fe_1 00 - xB_x (x = 14, 17, 20)$ alloys studied by electron diffraction and high-resolution electron microscopy, Phys. Rev. B **74**, 214206 (2006).
[46] G. H. Beall and L. R. Pinckney, Nanophase glass-ceramics, J. Am. Ceram. Soc. **82**, 5 (1999).
[47] C.-M. Lee, S.-W. Chae, H.-J. Kim, and J.-C. Lee, Role of nanocrystals on the plasticity of amorphous alloy, Met. Mater. Int. **13**, 191 (2007).
[48] Y. Hibino, T. Yamamoto, K. Yakushiji, T. Taniguchi, H. Kubota, and S. Yuasa, Highly energy-efficient spin-orbit-torque magnetoresistive memory with amorphous W-Ta-B alloys, Adv. Electron. Mater. **10**, 2300581 (2024).
[49] R. Gautam, S. Hiramoto, N. Kulesh, H. Mamiya, S. Okamoto, N. Ono, T. Ogasawara, T. Ohkubo, and H. Sepehri-Amin, Ultra-low core loss in Fe-enriched soft magnetic ribbons enabled by nanostructure and high-frequency domain engineering, Nat. Commun. **16**, 8022 (2025).
[50] K. Nishio, Dataset for "Metastability limit in the supercooled liquid state and its implications for glass formation and crystallization" [Data set], Zenodo, 2026, https://doi.org/10.5281/zenodo.23202643.